A strain-induced exciton transition energy shift in CdSe nanoplatelets
The impact of an organic ligand shell

Antanovich, Artsiom; Achtstein, A. W.; Matsukovich, A.; Prudnikau, Anatol V.; Bhaskar, P.; Gurin, V.; Molinari, M.; Artemyev, Mikhail

DOI
10.1039/c7nr05065h

Publication date
2017

Document Version
Accepted author manuscript

Published in
Nanoscale

Nanoscale

Accepted Manuscript

This article can be cited before page numbers have been issued, to do this please use: A. Antanovich, A. Achtstein, A. Matsukovich, A. Prudnikau, P. Bhaskar, V. Gurin, M. Molinari and M. Artemyev, *Nanoscale*, 2017, DOI: 10.1039/C7NR05065H.

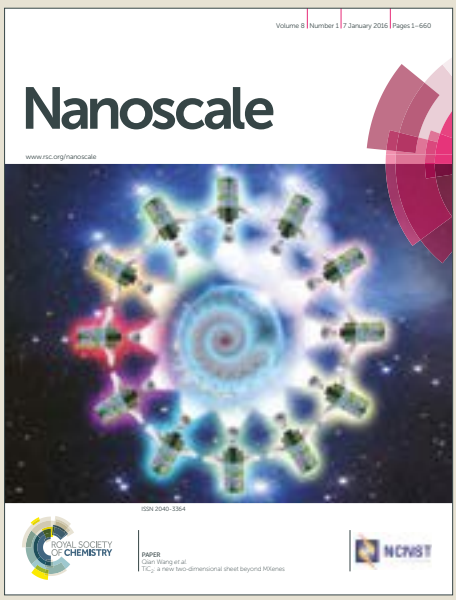

View Article Online
DOI: 10.1039/C7NR05065H

Journal Name

ARTICLE

Strain-Induced Exciton Transition Energy Shift in CdSe Nanoplatelets: The Impact of the Organic Ligand Shell

Received 00th January 20xx,
Accepted 00th January 20xx

DOI: 10.1039/x0xx00000x

www.rsc.org/

A. Antanovich,[a] A. W. Achtstein,[b] A. Matsukovich,[c] A. Prudnikau,[a] P. Bhaskar,[d] V. Gurin,[a] M. Molinari,[e] and M. Artemyev*[a]

We study the influence of surface passivating ligands on optical and structural properties of zinc blende CdSe nanoplatelets. Ligand exchange of native oleic acid with aliphatic thiol or phosphonic acid on the surface of nanoplatelets results in the large shift of the exciton transition for up to 240 meV. Ligand exchange also leads to structural changes (strain) in the nanoplatelet's core analysed by wide-angle X-ray diffraction. By correlating experimental data with theoretical calculations we demonstrate that the exciton energy shift is mainly caused by a ligand-induced anisotropic transformation of the crystalline structure altering the well width of the CdSe core. Further the exciton reduced mass in these CdSe quantum wells is determined by a new method and agrees well with expected values substantiating that ligand-strain induced changes in the colloidal quantum well thickness are responsible for the observed spectral shifts. Our findings are important for theoretical modeling of other anisotropically strained systems and demonstrate an approach to tune optical properties of 2D semiconductor nanocrystals over a broad region thus widening the range of possible applications of $A^{II}B^{VI}$ nanoplatelets in optics and optoelectronics.

Introduction

Ligands play a crucial role on the all stages of the colloidal nanocrystal (NC) lifecycle thus making studies of ligand-NC interactions highly important for practical application purposes.[1–6] At first, ligand molecules are used for the preparation of precursors for NCs synthesis and are also added to the reaction mixture to alter nucleation and growth kinetics, size, composition, morphology and crystalline structure of final nanoparticles.[7–17] Secondly, they stabilize nanoparticles by binding to their surface, thus lowering interface energy in a process of surface reconstruction and passivation of dangling bonds and vacancies.[5,18,19] Thirdly, different types of ligands are used to provide colloidal, chemical and photo-stability in various media and to engineer the NCs' reactivity, functionality and self-assembly.[1,2,4,20–27] And at last, due to the fact that significant portion of NCs atoms reside near or on the particle surface, ligands also have a great impact on physical properties (most notably optical properties) and determine NCs performance in various practical applications.[2,5,22,28] Moreover, native ligands (i.e. ligands that are left after the synthesis) in most cases could be relatively easily exchanged for other types of molecules without significant changes in the core composition to adjust physical and chemical properties of NCs for specific applications.[1–3,5]

Generally NCs' organic capping layers are considered as an analogue of self-assembled monolayers (SAMs), what allows extrapolation of the extensive information about the organic-inorganic interfaces on the interaction of ligands with NCs surfaces.[2,29] However, unlike SAM substrates such NCs as quantum dots (QDs) or nanorods possess highly curved surface faceted with different lattice planes and enriched with vertex and edge sites. Such difference affects ligand packing density, introduces disorder in the ligand layer and sometimes makes the data difficult to interpret unambiguously. In this aspect 2D semiconductor nanoplatelets (NPLs), like recently introduced CdSe ones, may become ideal candidates for studying the ligand-NC interface, since they have relatively large and atomically flat surface represented by only one type of crystalline planes – (100) in the case of zinc-blende (ZB) NPLs[30–32] and $(11\bar{2}0)$ in the case of wurtzite (WZ) ones.[31,33] Regardless of the recent advances in the synthesis[34–36] and investigation of optoelectronic properties[37–44] of both WZ and ZB NPLs, the knowledge of their surface chemistry remains scarce. At the same time, while surface chemistry of NPLs is expected to be similar to the surface chemistry of NCs of other dimensionalities, there are some insights that ligand passivation of NPLs has some unique features. For example,

[a] Research Institute for Physical Chemical Problems of the Belarusian State University, 220006 Minsk, Belarus. E-mail: m_artemyev@yahoo.com
[b] Institute of Optics and Atomic Physics, Technical University of Berlin, Strasse des 17. Juni 135, 10623 Berlin, Germany.
[c] B. I. Stepanov Institute of Physics, National Academy of Sciences, 220072 Minsk, Belarus.
[d] Department of Chemical Engineering, Delft University of Technology, Van der Maasweg 9, 2629 HZ, Delft, The Netherlands
[e] University of Reims Champagne Ardenne, Laboratory of Research in Nanosciences, LRN EA4682, 51685 Reims Cedex 2, France.

† Electronic Supplementary Information (ESI) available: Additional analytical description and calculation details, IR-spectra for 3.5 and 4.5 ML-thick NPLs capped with various ligands, TEM images, additional optical spectra and XRD data for 5.5 ML CdSe NPLs and stearic acid capped 3.5 ML-thick NPLs.

View Article Online
DOI: 10.1039/C7NR05065H

ligand passivation reduces the reactivity of basal planes, thus preventing an overcoating by an epitaxial shell with conventional methods,[45] but allowing two-dimensional growth and facilitating the formation of core-wings NPLs.[46,47] NPLs were also shown to self-assemble into layered columnar structures due to the interaction of their ligand shells. [48,49] In addition to that recently, we observed that the ligand exchange of native oleic acid layer on the surface of CdSe NPLs with aliphatic thiol or alkylphosphonic acids resulted in controlled self-assembly of NPLs into linear aggregates (stacks).[50]

In this paper we study in details how surface ligands exchange in ZB CdSe NPLs may affect their structural and optical properties. We demonstrate that different types of ligands can be used to alter the exciton transition energy of ZB CdSe NPLs by ligand-induced strain to the electronic system. This allows tuning their absorption edge by about 240 meV without changing their shape or chemical composition. Hence we introduce new ligand-assisted approach to control energies of excitonic transitions in colloidal 2D nanoparticles, which in principle could be transferred to other colloidal 2D systems like perovskites or transition-metal dichalcogenides (TMDs).

Experimental section

Materials and methods. Cadmium acetate dihydrate, zinc acetate dihydrate, cadmium oxide powder, selenium powder (100 mesh), oleic acid (OA), 1-octadecene, myristic acid, 1-hexadecanethiol (HDT) were purchased from Sigma-Aldrich. n-Hexadecylphosphonic acid (HDPA) was purchased from Plasmachem. Stearic acid (SA) was purchased from Merck. Chloroform, methanol and acetonitrile (analytical reagent grade) were purchased from Fisher Chemical. All reagents were used as-received without any further purification.

Optical absorption spectra were recorded using HR-2000+ spectrometer (Ocean Optics) equipped with Ocean Optics DH-2000 white light source. Photoluminescence measurements were conducted with Jobin-Yvon Fluoromax-2 spectrofluorimeter. TEM images were acquired using LEO 906E electron microscope. X-ray diffraction analysis of powdered samples was carried out with Empyrean Series 2 diffractometer (Cu Kα line). IR-spectra were recorded in the reflectance-absorption mode using Nexus (Thermo Nicolet) spectrometer equipped with Perkin Elmer Micro Specular Reflectance Accy-2x plate. Prior to XRD and IR measurements all samples were purified by several (not less than five) precipitation-dissolution cycles using chloroform as a solvent and methanol or acetonitrile as a non-solvent. After that the purified samples were dried and then grinded into a fine powder.

Preparation of CdSe nanoplatelets. CdSe NPLs with the thickness of 3.5, 4.5 and 5.5 monolayers (ML) were synthesized according to modified previously reported procedures.[38,51] Stearate-capped 3.5 ML-thick NPLs were synthesized by the same procedure as oleate-capped 3.5 ML-thick NPLs by replacing oleic acid in the starting mixture with stearic acid.

Results and discussion

In order to study the influence of different ligands on the optical and structural properties of ZB CdSe NPLs we exchanged oleate-ions on their surface for phosphonic acid and thiol. All these capping molecules bind to the surface as X-type ligands that irreversibly replace carboxylates in a two-step process involving proton exchange.[5,52–55] While hexadecylphosphonic acid is a much stronger ligand than oleic acid, the exchange process is fast and almost irreversible.[5,50,53,55] At the same time, since thiols are less acidic than carboxylic acids, the displacement of oleic acid with hexadecanethiol was performed in the presence of triethylamine, which acts as a deprotonating agent and facilitates formation of the thiolate-anion, which is more nucleophilic and forms strong bonds with CdSe surface.[50,54,56]

Ligand exchange process was monitored using IR- and optical spectroscopy. Changes observed on IR-spectra upon ligand exchange (see Figure S1 in the ESI†) were consistent with the results of the analysis from our previous report,[50] i.e. characteristic features of carboxylic acid disappeared upon the addition of phosphonic acid or thiol, while new features attributable to phosphonates and thiolates appeared, thus confirming ligand exchange process. Resulting absorption and PL spectra of starting and ligand-exchanged NPLs in chloroform solutions are presented in Figure 1.

View Article Online
DOI: 10.1039/C7NR05065H

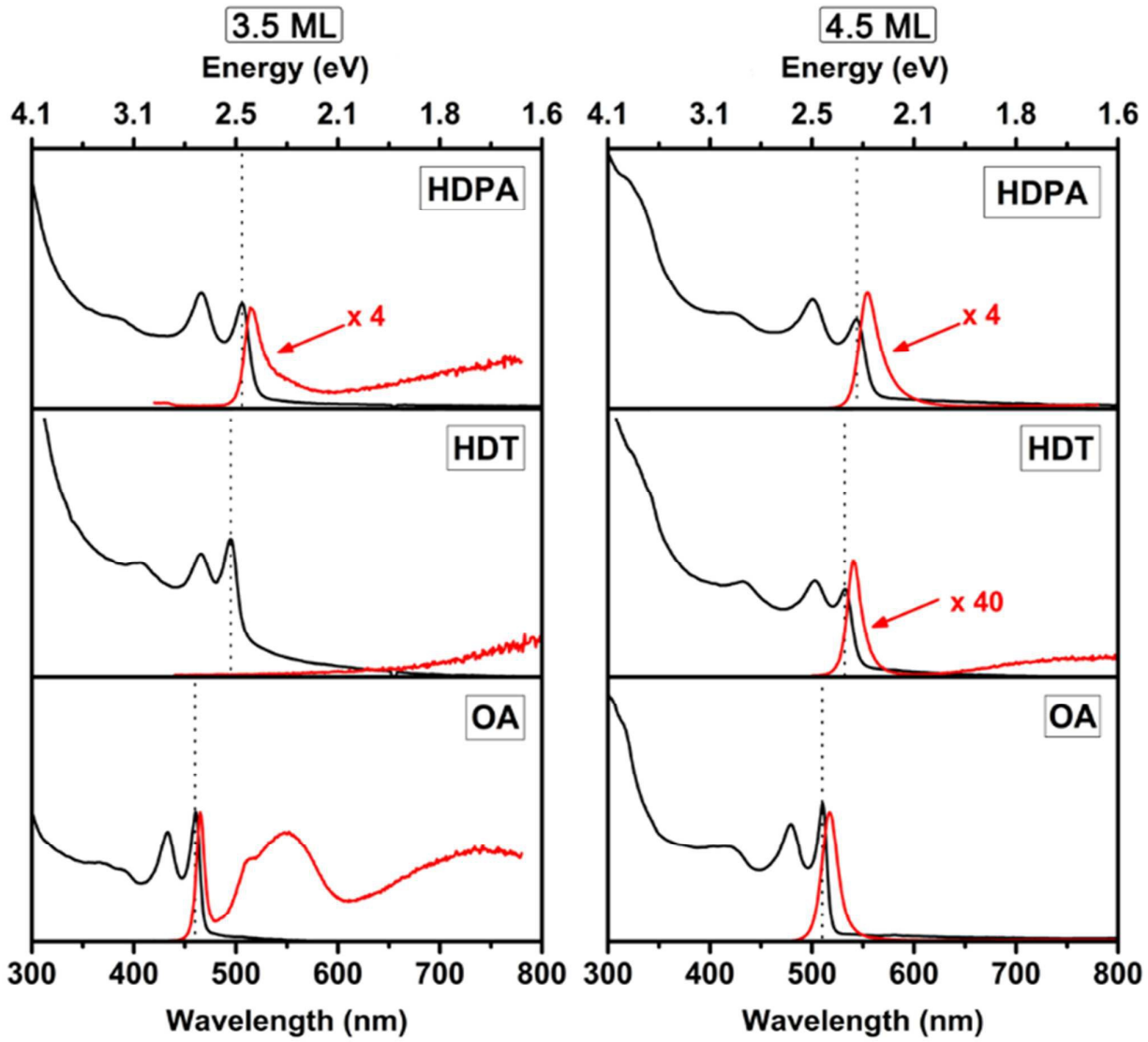

Figure 1 – Absorbance (black) and PL (red) spectra of 3.5 ML- (left) and 4.5 ML-thick (right) CdSe NPLs capped with oleic acid (OA), hexadecanethiol (HDT) and hexadecylphosphonic acid (HDPA). PL spectra of 3.5 ML- and 4.5 ML-thick NPLs were recorded upon excitation at λ=400 nm and 450 nm respectively. Dotted lines indicate the position of the first absorption maxima.

It can be seen that upon ligand exchange with HDT and HDPA optical spectra become considerably red-shifted by up to ~240 meV. Upon exchange of native oleic acid with thiols PL of the NPls is considerably quenching similarly to CdSe NCs of other shapes.[57] Less pronounced quenching resulting in a QY of 6-8 % in the case of HDPA might be explained by the disorder in the ligand shell accompanying the ligand exchange process, since the PL QY of HDPA-coated NPls slowly increases during their storage in solution (the PL QY for initial OA-capped NPls is about 25%). The QY maybe therefore increased again by appropriate post ligand exchange treatment. The broadening and asymmetric shape of PL bands in case of HDT and HDPA ligands is most probably related to the formation of shallow traps during the ligand exchange and potentially an alteration of the dephasing and corresponding homogeneous linewidth. It is also interesting to note that in absorption the hh – lh intensity ratio decreases by trend from OA to HDPA ligands in Figure 1. This may either be related to a change of the radiative and pure dephasing rates, altering the emission linewidth for the hh and lh differently. Alternatively a change of the hh continuum,[58] which lies under the lh peak and the hh exciton transition strength may cause the trend, as their and the lh exciton absorption strength depends on the actual well width. The observed tendential increased broadening of the hh PL emission for HDPA samples is an argument for the first variant. These findings may stimulate modelling beyond the scope of this article to clarify the underlying processes.

Similar, but much less pronounced ligand-induced spectral shifts were reported for QDs.[55] Large red-shifts by 10-40 nm were observed for less conventional capping ligands such as phenylchalcogenols Ph-X (X = SH, SeH, TeH).[59] Even larger spectral changes (up to 220 meV) have been reported for so-

View Article Online
DOI: 10.1039/C7NR05065H

called "non-innocent" ligands (i.e. ligands that introduce new electronic states[2]) such as conjugated phenyldithiocarbamates.[60] Both these types of ligands reduce NCs' band gap by delocalizing holes of the exciton and thus decreasing the quantum confinement in the core. However, conventional ligands as the ones used in the current work generally alter the confinement and exciton transition energies by changing the valence and conduction band offsets of the semiconductor nanoparticles only to a limited extent. These changes are relatively low,[55] as the HOMO-LUMO gaps of these organic ligands (e.g. oleic acid) are all close to ~ 8 eV.[61–63] Recently Zhou et. al [64] reported large (up to 140 meV) spectral shifts upon reversible exchange of amines (L-type ligands) for Cd- or Zn-carboxylates (Z-type) in another family of 2D cadmium chalcogenides – so-called quantum belts. Unlike ZB NPls quantum belts have wurtzite crystalline arrangement and their both top and bottom sides are terminated with nonpolar $(11\bar{2}0)$ planes exposing both cadmium and selenium atoms.[31,33,35] Observed red shifts were in part explained by the relaxation of quantum confinement, due to the binding of extra cadmium species to surface chalcogen atoms and growth of the additional Cd layer, what can be considered as an increase in quantum belt thickness.

Unlike in WZ quantum belts, basal planes of ZB NPLs are terminated with Cd atoms on both sides and covered with X-type carboxylates that act as a potential barrier.[30,31] While spectral shifts upon HDT capping might be explained by the growth of an additional sulfide quasi-layer[65] and subsequent lowering of the spatial confinement, an even larger red-shift upon HDPA treatment could not be rationalized in the same manner, as in the case of HDPA no additional sulfur atomic layer is formed. Thus, in order to explain the origin of the observed changes of exciton transition energy, additional factors need to be addressed.

Alternatively, large spectral shifts can be related to the changes in local dielectric environment, as the energy levels in CdSe NPLs were shown to be very sensitive to the dielectric environment.[39] However since high frequency dielectric constants of most organic ligand molecules are around 3,[39] the impact of the changes in dielectric confinement is too low to explain observed spectral shifts on the order of the exciton binding energy (~ 200 meV [39,66]) presented in Figure 1.

Therefore a possible influence of the ligand exchange-induced structural changes is considered. It has been shown that lattice strain can alter the energy levels in core and core-shell NCs.[64,67–69] While ligands on the surface of QDs were reported to cause both lattice contraction and expansion relatively to the bulk phase,[64,70,71] to the best of our knowledge, information on the interplay between spectral characteristics and ligand-induced strain in 2D semiconductor nanoparticles remains scarce.[64]

In order to monitor changes of the lattice parameters of ZB

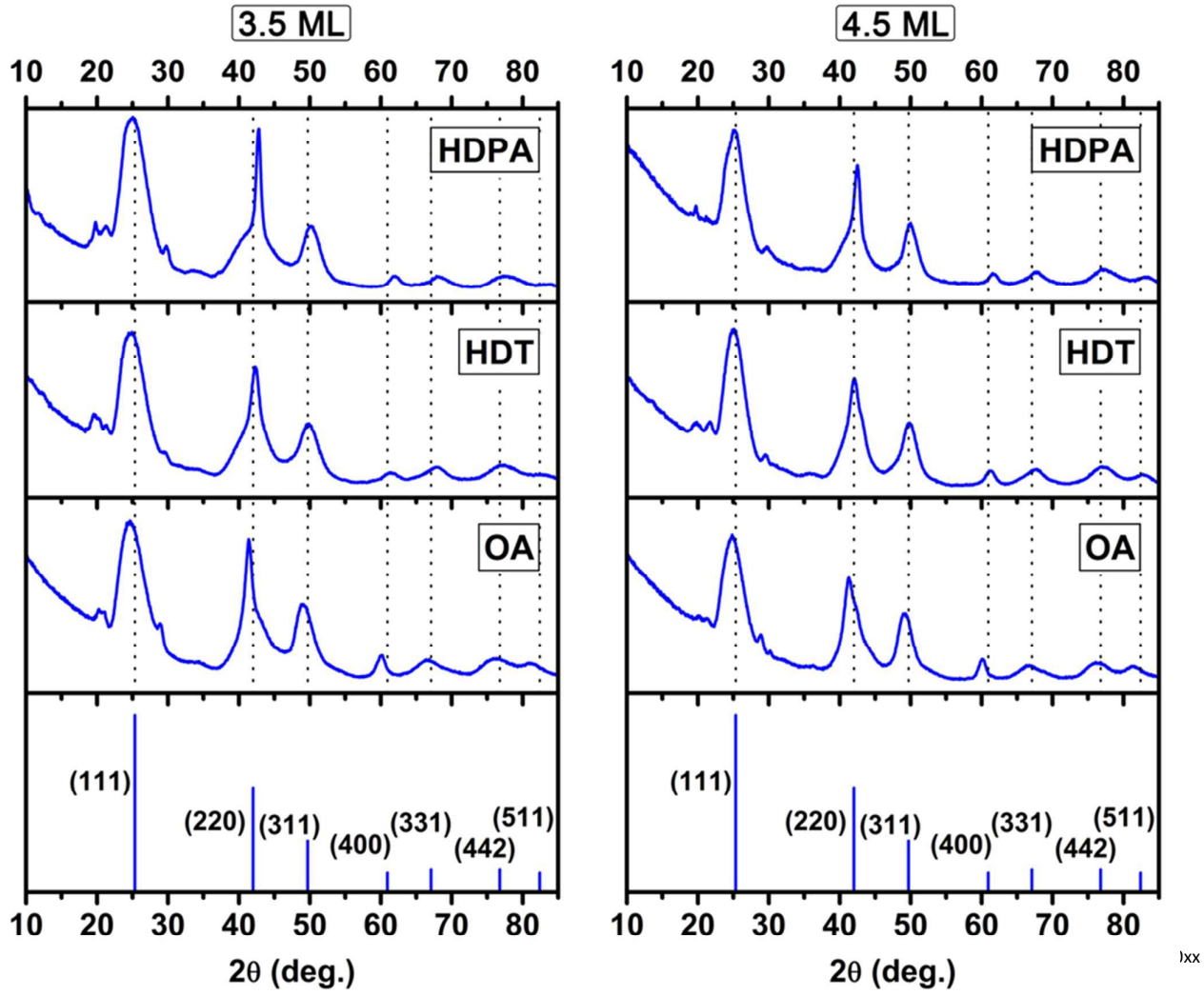

Figure 2 – Wide-angle XRD diffractograms of 3.5 (left) and 4.5 (right) ML-thick CdSe NPLs capped with oleic acid (OA), hexadecanethiol (HDT) and hexadecylphosphonic acid (HDPA). Bar graphs and dotted lines indicate values for bulk ZB CdSe phase.

View Article Online
DOI: 10.1039/C7NR05065H

CdSe NPLs we performed wide-angle XRD measurements. X-ray diffractograms obtained for powders of ligand-exchanged NPLs are presented in Figure 2. Consistently with previous reports XRD-diffractograms of oleic acid-capped 3.5 ML and 4.5 ML NPLs exhibit reflexes characteristic for ZB crystalline lattice.[30,31,72] After the ligand exchange with HDT and HDPA the diffractograms of NPLs still have the same ZB peaks, thus suggesting that no recrystallization takes place and that NPLs retain their ZB lattice. However, upon closer examination it becomes clear that positions of the peaks vary for NPLs capped with different ligands.

Earlier studies of carboxylate-capped NPLs suggested that their crystalline lattice is slightly distorted, what results in the appearance of forbidden (110) and (200) reflexes around 2θ = 20 ° and 28 °, respectively, and splitting of the (220) reflex into broad and sharp features.[30,31] Such splitting was attributed to the non-uniform deformation of NPLs observed by HRTEM and explained by the fact that these peaks arise from planes of the same family that lie in the lateral and thickness directions.[30] Since the FWHM of reflexes tends to increase as the nanoparticle size decreases, differences in the peak width may be attributed to a difference in NPLs size in lateral (up to tens of nm) and thickness (~ 1.0 - 1.5 nm) directions. Thus it is possible to attribute the sharp peak to the diffraction on planes perpendicular to the NPLs basal planes (red-colored in Figure 3) and the broad one – to the diffraction on crystalline planes that are more oriented to the thickness direction (blue-colored in Figure 3).

In order to study this effect in more detail and determine NPLs' lattice parameters, we closely examined the obtained diffractograms in the region of 2θ = 35 – 50 ° and fitted the XRD peaks with Voigt functions[30,73] using Fityk software.[74] The interplane distances related to the (220) planes in thickness and lateral directions and corresponding lattice parameters were calculated on the basis of the position of maxima of the fitted (220) peaks (Figure 4). Lattice parameters were calculated only on the basis of the (220) peak, since only these peaks demonstrate clear splitting, which allows unambiguous attribution of the reflexes to planes that lie in different directions, whereas other peaks do not show such splitting due to their unfavorable relative orientation to NPLs basal planes, e.g. (311) reflex (some additional calculation details are provided in the ESI†).

Figure 4 shows that peak shifts, broadening and splitting are more pronounced for 3.5 ML-thick NPLs due to their smaller thickness and due to the fact that 3.5 ML-thick NPLs grow faster and their synthesis usually produces NPLs with large lateral dimensions (tens of nm) in comparison to 4.5 ML-thick NPLs, which usually have smaller lateral size and a more uniform rectangular shape (see Figure S2 in the ESI†). Results of structural data analysis for all three types of CdSe NPLs (3.5, 4.5 and 5.5 ML) are summarized in Table 1 (corresponding optical spectra and XRD diffractograms for 5.5 ML CdSe NPLs are presented in the ESI† in Figure S3 and Figure S4 respectively).

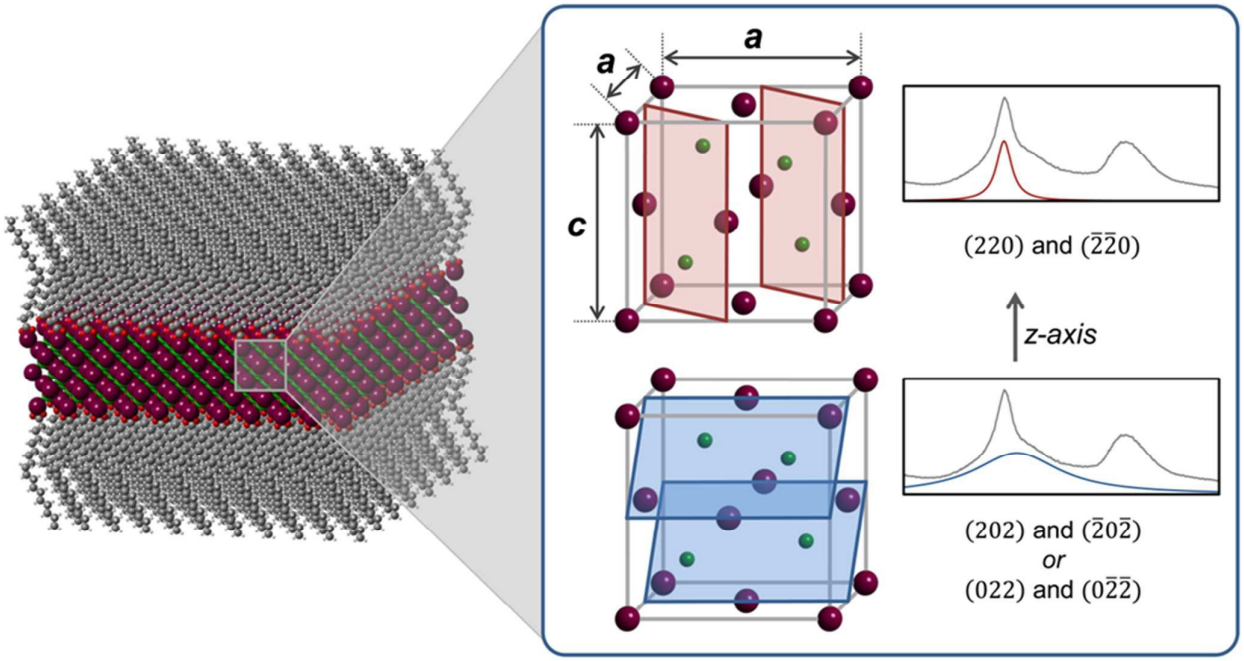

Figure 3 – Scheme demonstrating tetragonal lattice distortion in CdSe NPLs and the origin of the XRD-peak splitting.

Table 1 – Structural data of CdSe nanoplatelets with different ligands: interplane distance as obtained from the (220) reflexes, tetragonal lattice parameters, relative parameter change and unit cell volume.

Sample	d_{220}, Å	d_{220}, Å	a, Å	c, Å	a/c	$\Delta\varepsilon_{x,y}$, %[a]	$\Delta\varepsilon_{z}$, %[a]	V, Å^3

View Article Online
DOI: 10.1039/C7NR05065H

	lateral	thickness						
3.5 ML OA	2.182	2.154	6.17	6.02	1.026	0	0	229.2
3.5 ML HDT	2.134	2.163	6.03	6.20	0.973	-2.19	3.11	226.0
3.5 ML HDPA	2.119	2.167	5.99	6.27	0.955	-2.89	4.30	225.4
4.5 ML OA	2.188	2.143	6.19	5.94	1.042	0	0	227.6
4.5 ML HDT	2.145	2.148	6.07	6.08	0.997	-1.97	2.39	223.9
4.5 ML HDPA	2.127	2.160	6.02	6.21	0.969	-2.79	4.47	224.7
5.5 ML OA	2.183	2.149	6.17	5.98	1.031	0	0	228.2
5.5 ML HDT	2.155	2.150	6.09	6.07	1.005	-1.28	1.35	225.4
5.5 ML HDPA	2.129	2.161	6.02	6.21	0.970	-2.47	3.68	225.1

[a] Lattice strain Δε was calculated with respect to corresponding 3.5, 4.5 and 5.5 ML OA-capped NPLs.

Figure 4 and Table 1 demonstrate that ligand exchange in all 3.5, 4.5 and 5.5 ML-thick NPLs causes structural changes that follow the same trend. Also as indicated by the value a/c, NPLs experience tetragonal deformation in the order of OA-HDT-HDPA involving shrinkage in the lateral direction and expansion in the thickness direction (with respect to OA). Such lattice distortions upon ligand exchange are schematically shown in Figure 5.

In principle lattice distortions may be attributed to multiple factors such as strain induced by the van der Waals attraction or steric repulsion of ligand hydrocarbon tails, surface reconstruction induced by ligand headgroups or different ligand packing density. McGuiness et al. observed a lattice rearrangement of e.g. a (001) GaAs surface induced by the

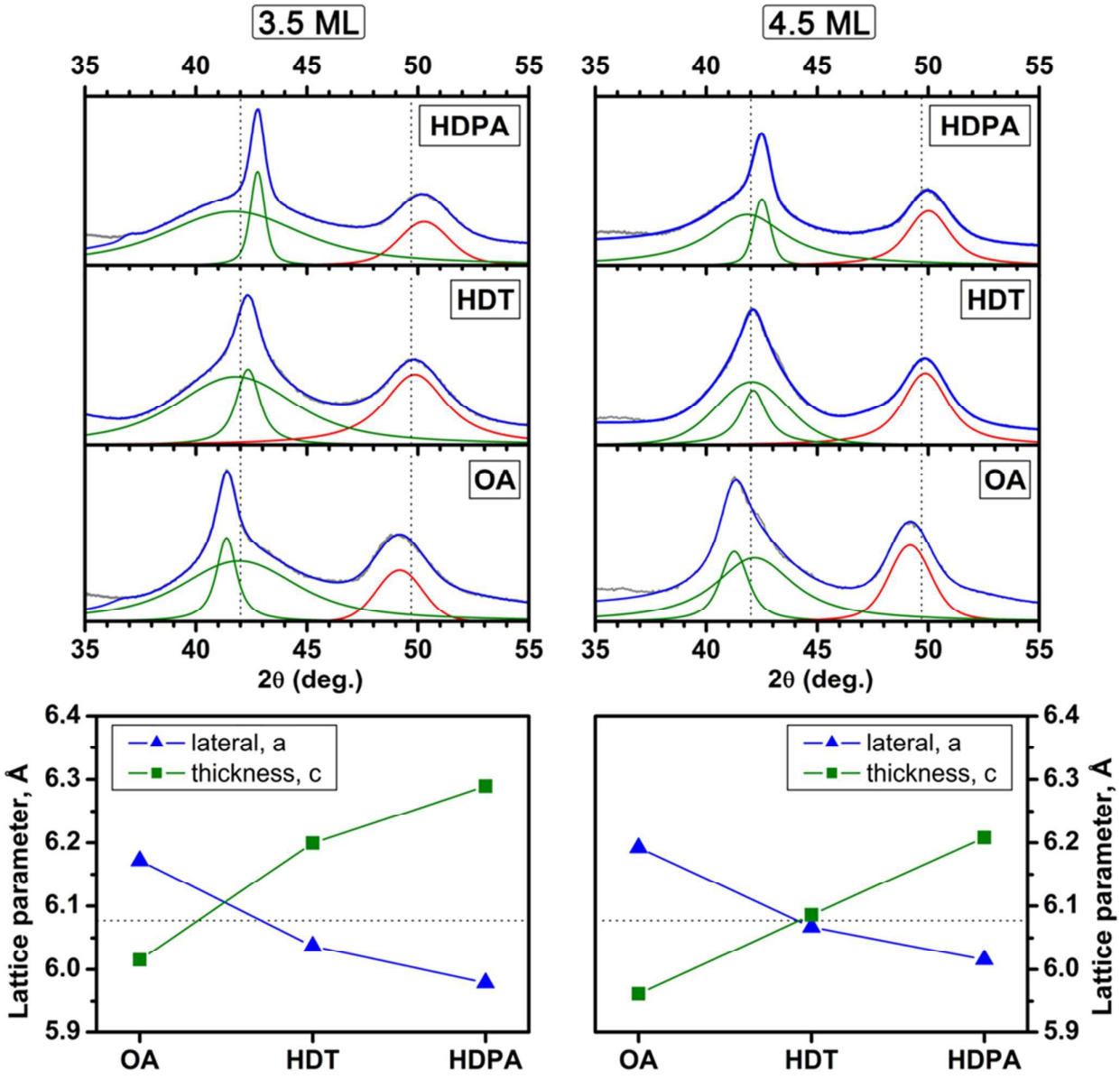

6 | Figure 4 – Results of the fitting of (220) and (311) XRD peaks for 3.5 and 4.5 ML-thick CdSe NPLs. Grey curve – experimental data, green – fitted peaks for (220) reflexes, red – fitted peaks for (311) reflexes, blue – cumulative curve (top) and variation of lattice parameters in different directions for 3.5 ML and 4.5 ML-thick NPLs treated with different ligands (bottom). Dotted lines indicate corresponding values for bulk ZB CdSe phase.

View Article Online
DOI: 10.1039/C7NR05065H

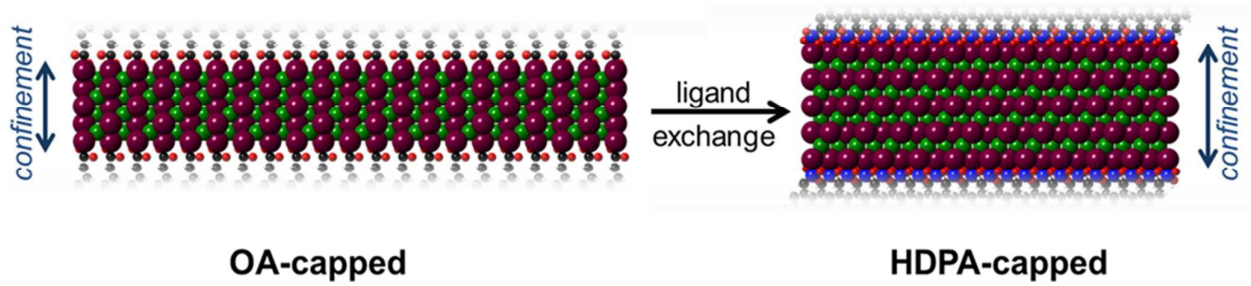

Figure 6 – Scheme demonstrating anisotropic lattice transformations upon ligand exchange. Ligand hydrocarbon tails are omitted for clarity. Drawings are not to scale; the extent of changes is exaggerated for demonstration.

formation of a thiol SAM on the interface.[75] Lattice mismatch between the alkanethiolate layer and underlying GaAs substrate caused there a contraction of GaAs surface in order to maximize the van der Waals interaction of the ligands. In addition to that, in our recent paper [50] it was shown on the basis of IR-spectroscopy data that due to dispersive interligand interaction, ligands with saturated alkyl chains (such as SA, HDT or HDPA) tend to form ordered layers with ligand tails being in all-trans conformation, whereas OA ligand layers do not exhibit such ordering. This difference was attributed to the ligand-ligand interaction governed by the geometry of alkyl chains. Since in comparison with SAMs NPLs have small finite sizes, one may expect that ligand-induced lattice distortions in NPLs may be more pronounced.[70] Additionally, several groups reported that ligand-induced surface reconstruction propagates over several crystalline layers below the NC surface.[18,76] Considering the small thickness of NPLs and their finite surface area, it may be assumed that structural changes could affect the whole particle. The opposite direction of lattice changes (e.g., contraction in the lateral direction accompanied by the expansion in the thickness direction) can be understood as a way to redistribute the ligand-induced strain in the crystalline lattice (see Figure 5).

In order to check whether the lattice rearrangement is caused by the interligand van der Walls interaction, we compared the lattice parameters of OA- and SA-capped 3.5 ML-thick NPLs. To do this we synthesized 3.5 ML-thick NPLs using cadmium stearate instead of cadmium oleate as a Cd-source. Representative XRD-diffractograms and their fits are shown in Figure 6. Fitting of (220) peaks yields almost the same interplane distances and lattice parameters (see Tables 1 and S2 in the ESI†). At the same time absorption and PL spectra of SA-capped NPLs (see Figure S5 in the ESI†) are also almost identical to those of OA-capped NPLs. These results suggest that the geometry of the alkyl chain of capping ligands does not affect NPLs' crystalline structure relevantly.

Thus it can be assumed that the interaction of ligand tails in the case of NPLs is significantly reduced in comparison to SAMs and is primarily governed by the underlying CdSe surface. This assumption is in line with several reports that suggest that even in SAMs strong binding of functional groups to the interface makes disorder in the headgroup bonding less favourable than disorder in organic layer,[77–79] thus suggesting that in such cases the underlying crystalline lattice determines ligand packing densities but not vice versa.

The nature of the observed lattice transformations is not yet clearly understood and is believed to be of complex nature with the contributions of multiple competing factors.

Earlier, Rockenberger et al. observed lattice shrinkage in thiol-capped CdTe nanoclusters that was attributed to the length

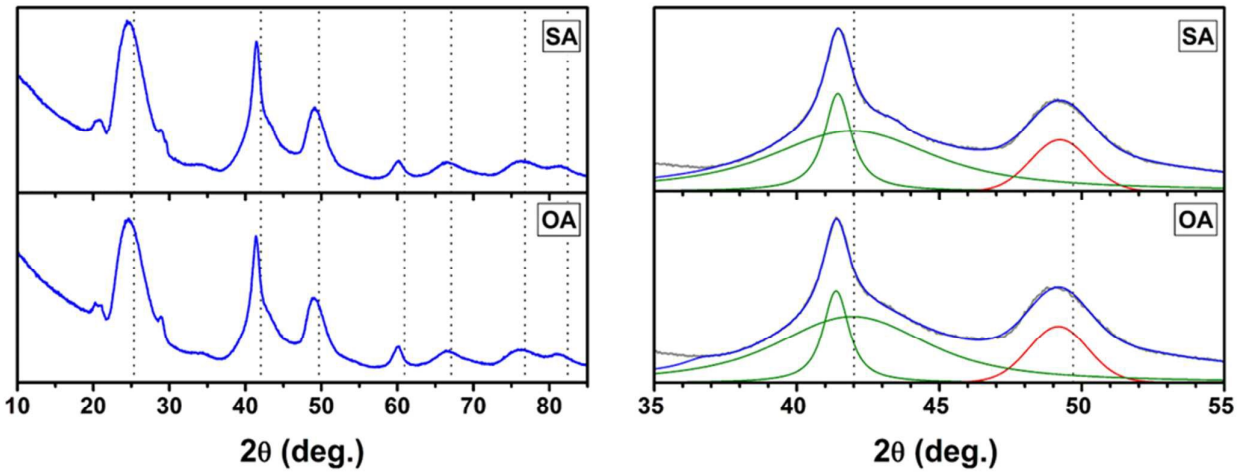

Figure 5 – Wide -angle XRD-diffractograms (left) and corresponding fits (right) of SA- and OA-capped 3.5 ML-thick CdSe NPLs. Grey curve – experimental data, green – fitted peaks for (220) reflexes, red – fitted peaks for (311) reflexes, blue – cumulative curve. Dotted lines indicate corresponding values for bulk ZB CdSe phase.

View Article Online
DOI: 10.1039/C7NR05065H

mismatch of Cd-Te bonds in the core with Cd-S bonds on the particle interface.[70] On the other hand, several reports indicate that the average thiol coverage in CdSe NCs is larger than the coverage by phosphonates and carboxylates (~ 5 nm^{-2} vs ~ 3-4 nm^{-2}).[3,53,55,80] It was attributed to monodentate binding of thiols with surface atoms and to the fact that upon ligand exchange some thiol molecules not only displace native carboxylates but also bind to free non-passivated sites on the surface.[55] Such increase of ligand coverage is likely to result in the increase of repulsive interaction of thiol headgroups, thus causing tensile strain. The interplay of these two factors explains the decrease of lattice constant comparatively to OA and less pronounced lattice shrinkage in comparison to HDPA. While compressive in-plane strain in HDPA-coated NPLs may also be rationalized in the same manner, especially considering reduced average ligand coverage in comparison to thiol and shorter Cd-O bonds in cadmium phosphonates in comparison to cadmium carboxylates (2.1 – 2.3 Å vs 2.3 – 2.7 Å), [81–84] additional factors could also be relevant. At first, several reports show that phosphonic acids replace carboxylates in a 1:1 stoichiometry, therefore suggesting that phosphonic acid binds as a hydrogen phosphonate RPO_3H^-, [53,55] thus leaving the possibility for interligand attraction due to the formation of hydrogen bonds.

To gain more insight into the effects of ligand-induced strain to the nanoplatelets, we analysed the influence of lattice rearrangement on the band gap of the NPLs. Since XRD measurements were carried out using powdered samples and optical spectra were recorded in the solution we compared both. We acquired absorption and PL spectra of the powders of 3.5 ML-thick NPLs used for XRD (see Figure S6 in the ESI) as well as in solution. The absorption spectra of powder samples were made from their slurry in commercial silicon-based immersion oil for microscopy (the details of procedure are described in the caption to Fig. S6). Since the energies of the first excitonic transitions of NPLs in powder and in solution are almost the same, both for PL and absorption, we can conclude that drying did not alter NPLs' bandgap significantly (with respect to the much larger strain induced shifts upon ligand exchange) and we can correlate optical data acquired in NPLs solution with lattice parameters obtained using XRD.

CdSe nanoplatelets were shown to be terminated with Cd atoms on the both sides[30,31] what leads to a net charging of the CdSe core platelets without surface ligands, as every terminal Cd atom carries a non-compensated net charge of Q_e. This is due to the fact that Cd-terminated NPLs are nonstoichiometric, and charge compensation can therefore be accomplished by the negatively charged ionic species on their surface. As the density of terminal Cd atoms is determined by CdSe ZB structure and does not necessarily match the interchain spacing of the surface ligands in SAM, ligand headgroup interaction with surface Cd atoms introduces lattice strain. This strain is expected to result in a change of excitonic band gap of CdSe NPLs, which is either due to a deformation caused by the distortion of the unit cell or a strain-induced change of the well thickness and hence the exciton confinement.

At first we considered possible correlation between ligand-induced lattice deformation and the observed exciton energy shifts. As upon ligand exchange not only in-plane compression, but also perpendicular expansion is observed (Table 1), it is possible to calculate energy shifts with respect to OA-capped NPLs using the hydrostatic deformation potential. Applying a model for hydrostatic as well as biaxial strain (equation S7) and an approach involving the Youngs modulus (equation S8) the calculated NPL band gap shifts ($\Delta E_{calc}^{(S7)}$ and $\Delta E_{calc}^{(S8)}$ with respect to the case of oleic acid capped platelets) are presented below in Table 2. [85,86] (see ESI for details). Analyzing the results we see that still a much smaller blue shift is predicted in the first case ($\boldsymbol{\Delta E_{calc}^{(S7)}}$) in contrast to the observed large red shift. Hence deformation potentials can account for only <20 % of the observed shift, and are hence a small perturbation. In the case of equation S8 a redshift is predicted, however the predicted values are approximately 2-3 times lower than the experimentally observed values, so both approaches do not explain the experimental findings. This discrepancy can be attributed to the major drawback of such calculations as they are based on theory for an isotropic bulk solid, which does not take into account changes of parameters upon the transition from bulk solids to quantum confined 2D nanoparticles and the resulting impact on elastic constants, deformation potentials, the quantum confinement energies etc.

Table 2 – Experimental and calculated exciton energy shifts for CdSe NPLs

Sample	ΔE_{exp}, meV [a]	$\Delta E_{calc}^{(1)}$, meV [a]	$\Delta E_{calc}^{(S7)}$, meV [a]	$\Delta E_{calc}^{(S8)}$, meV [a]
3.5 ML OA	0	0	0	0
3.5 ML SA	- 6	-8.4	1.5	-2.2
3.5 ML HDT	- 191	-180	23	-52
3.5 ML HDPA	- 245	-239	31	-72
4.5 ML OA	0	0	0	0
4.5 ML HDT	- 102	-88	21	-40
4.5 ML HDPA	- 149	-153	30	-75
5.5 ML OA	0	0	0	0
5.5 ML HDT	- 46	-34	14	-23
5.5 ML HDPA	- 112	-86	26	-62

[a] The heavy-hole exciton transition energy for capping with oleic acid has been taken as the reference zero point. For calculations using Eq. (1) the value of μ = 0.105 m_0 was used (as taken from theory (Ref. [87]) and reasoned in the main text).

In order to investigate the impact of the anisotropic one-dimensional confinement in the platelets, we estimated changes in transversal confinement energy of a quantum well (CdSe NPLs) upon small thickness changes due to ligand-induced lattice deformation. For simplicity, we assumed an infinite deep quantum well with reduced exciton mass μ. Energetic shifts of the confinement energy with respect to corresponding OA-capped NPLs are calculated using the standard expression of the confinement energy of an infinitely deep well:

$$\Delta E = \frac{\pi^2\hbar^2}{2\mu}\left(\frac{1}{L_{z,x}^2} - \frac{1}{L_{z,OA}^2}\right), \qquad (1)$$

View Article Online
DOI: 10.1039/C7NR05065H

where $L_{z,x}$ and $L_{z,OA}$ are the thicknesses of NPLs capped with ligand x and OA, respectively. The NPL thickness was calculated using the following equation:[44]

$$L_z = c \cdot 0.5 \cdot N, \qquad (2)$$

where c is the lattice parameter for corresponding NPLs from Table 1 and N is the number of monolayers in NPLs (3.5, 4.5 or 5.5 ML). $L_{z,OA}$ is the reference well width of 3.5, 4.5 or 5.5 ML-thick OA-capped CdSe nanoplatelets. Hence, we consider the ligand exchange as a perturbation with respect to oleic acid-covered platelets of the same thickness. Transition energy shifts $\Delta E_{calc}^{(1)}$ calculated using Equation 1 are summarized in Table 2.

A quite good agreement of the observed spectral shifts with the predictions made using quantum well model can be observed. Comparing the observed redshifts with the increase of the transversal lattice parameter c in Table 1 it becomes evident that an increase in the well width leads to the redshift of the exciton transition in CdSe nanoplatelets according to equation (1).

To definitely prove that ligand-induced changes in well width are the reason for observed experimental red shifts, we use a correlation plot, where excitonic shifts observed in the experiment (ΔE_{exp} from Table 2) are plotted versus $\left(\frac{1}{L_z^2} - \frac{1}{L_{z,OA}^2}\right)$ in Figure 7.

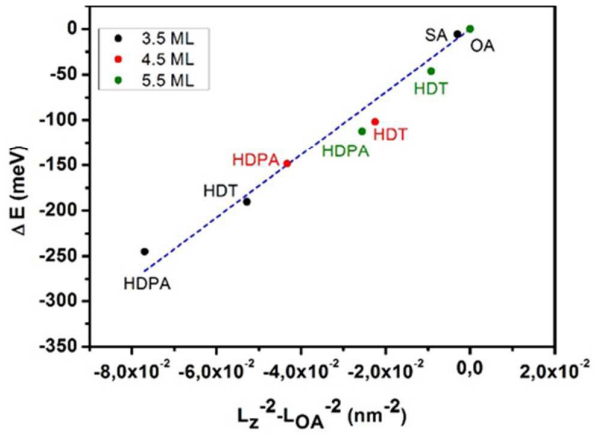

Figure 7 - Energetic shifts of the exciton transitions in CdSe nanoplatelets versus the difference of the inverse well width squared with respect to OA-capped NPLs. The dashed line represents a linear fit of all points. Values for 3.5, 4.5 and 5.5 ML OA coated (reference) platelets lay on top of each other on the uppermost left point.

As expected from Equation 1, a linear dependency is observed. A linear fit, yielding an R^2 of 0.98, shows the excellent agreement of the experimental shifts with respect to OA with the model in Equation 9. From the slope the exciton reduced mass μ, which corresponds to the effective electron and hole masses in perpendicular direction to the well, can be deduced. We obtain μ = 0.104 ± 0.005 m_0 which is in very good agreement with the expected perpendicular reduced exciton mass in ZB CdSe, calculated using Luttinger parameters from Ref. [88] and their relation to the out-of-plane heavy hole mass $m_{hh} = m_0/(\gamma_1 - 2\gamma_2)$[87] and the electron mass. This results in an expected reduced mass of μ = 0.105 ± 0.01 m_0, in excellent agreement with the experimental result. Hence the observed ligand-induced redshifts in the CdSe NPLs are shown to be related to a ligand induced alteration of the semiconductor quantum well width. So the ligand-induced compressive in-plane strain results in a transversal expansion, as we change the ligands from OA to HDPA.

On the other hand the correlation plot in Figure 7 using Equation 1 represents a new method to determine the exciton reduced mass in colloidal quantum wells via correlating the observed ligand-induced spectral shifts to the changes in the lattice parameters (and subsequently well width) determined by XRD.

The ligand-induced spectral shifts of the quantum well heavy hole exciton transition have a strong influence on the electronic properties and have to be taken into account in all modelling of colloidal ligand-capped 2D semiconductor nanocrystals, e.g. by k·p or tight-binding approaches, as ligand-induced strain strongly alters transition energies (by up to ~240 meV in the case of CdSe NPLs). Another notable consequence of the anisotropic distortion of the unit cell by ligands (as indicated by a/c parameters in Table 1) is that the cubic symmetry of the ZB CdSe lattice is reduced to tetragonal symmetry. Therefore high optical nonlinearities can be expected, what is in line with observations of high two-photon absorption cross-sections of the CdSe NPLs, which are enhanced well above the shape-associated effects of local fields.[89]

Conclusions

In this paper we have demonstrated that upon ligand exchange of oleic acid by hexadecanethiol and hexadecylphosphonic acid on the surface of ZB CdSe NPLs the latter experience large red shifts of the excitonic transition energies for up to 240 meV. By the means of XRD it was shown that capping of CdSe NPLs with organic ligands leads to a considerable distortion of the zinc blende unit cell. Upon ligand exchange with HDT and HDPA lateral contraction of the lattice leads to a perpendicular expansion of the quantum well. This interpretation was substantiated by deducing the reduced exciton mass in a quantum well by correlating experimental spectroscopic shifts with the well width changes determined from XRD data. The magnitude of the strain induced excitonic transition energy shift is related to the well width changes and determined by ligand type, primarily the head group, and NPL thickness. Energy shifts calculated using deformation potentials are shown to be only a fraction of the experimentally observed spectral changes.

Current observations open up a possibility to tune heavy hole exciton transition energies in CdSe NPLs, normally situated around ~3.22 eV, ~2.67 eV, ~2.4 eV and ~2.23 eV [44,72] for up to ~ 240 meV over nearly the whole visible range, thus making them interesting candidates for e.g. lighting or display technology. Due to the breakup of the isotropic inversion

View Article Online
DOI: 10.1039/C7NR05065H

symmetry in the originally face-centered (ZB) crystal structure, high optical nonlinearities are expected to occur in CdSe NPLs.

Acknowledgements

A.W.A. acknowledges DFG project AC 290/1+2. A.P. and V.G. acknowledge financial support from CHEMREAGENTS program. A.A. acknowledges partial financial support from Belarusian republican foundation for fundamental research (grant X16M-020). M.A. and M.M. thanks the region Champagne Ardenne for their support via its "International invited professor program". We would like to thank A. Karoza for help with IR-spectroscopy and K. Skrotskaya for TEM investigation.

Notes and references

1 R. Brutchey, Z. Hens and M. V. Kovalenko, in *Chemistry of Organo-Hybrids*, John Wiley & Sons, Inc., Hoboken, NJ, USA, 2015, pp. 233–271.
2 M. A. Boles, D. Ling, T. Hyeon and D. V. Talapin, *Nat. Mater.*, 2016, **15**, 141–153.
3 A. J. Morris-Cohen, M. Malicki, M. D. Peterson, J. W. J. Slavin and E. A. Weiss, *Chem. Mater.*, 2013, **25**, 1155–1165.
4 H. Mattoussi, G. Palui and H. Bin Na, *Adv. Drug Deliv. Rev.*, 2012, **64**, 138–166.
5 J. De Roo, K. De Keukeleere, Z. Hens and I. Van Driessche, *Dalt. Trans.*, 2016, **45**, 13277–13283.
6 D. V. Talapin, J.-S. Lee, M. V. Kovalenko and E. V. Shevchenko, *Chem. Rev.*, 2010, **110**, 389–458.
7 Z. A. Peng and X. Peng, *J. Am. Chem. Soc.*, 2001, **123**, 183–184.
8 R. García-Rodríguez and H. Liu, *J. Am. Chem. Soc.*, 2014, **136**, 1968–1975.
9 R. García-Rodríguez, M. P. Hendricks, B. M. Cossairt, H. Liu and J. S. Owen, *Chem. Mater.*, 2013, **25**, 1233–1249.
10 N. T. K. Thanh, N. Maclean and S. Mahiddine, *Chem. Rev.*, 2014, **114**, 7610–7630.
11 L. Liu, Z. Zhuang, T. Xie, Y. Wang, J. Li, Q. Peng and Y. Li, *J. Am. Chem. Soc.*, 2009, **131**, 16423–16429.
12 Y. Gao and X. Peng, *J. Am. Chem. Soc.*, 2014, **136**, 6724–6732.
13 G. H. V. Bertrand, A. Polovitsyn, S. Christodoulou, A. H. Khan and I. Moreels, *Chem. Commun.*, 2016, **52**, 11975–11978.
14 S. Sun, D. Yuan, Y. Xu, A. Wang and Z. Deng, *ACS Nano*, 2016, **10**, 3648–3657.
15 A. Pan, B. He, X. Fan, Z. Liu, J. J. Urban, A. P. Alivisatos, L. He and Y. Liu, *ACS Nano*, 2016, **10**, 7943–7954.
16 M. S. Bakshi, *Cryst. Growth Des.*, 2016, **16**, 1104–1133.
17 R. S. Koster, C. Fang, A. van Blaaderen, M. Dijkstra and M. A. van Huis, *Phys. Chem. Chem. Phys.*, 2016, **18**, 22021–22024.
18 M. G. Berrettini, G. Braun, J. G. Hu and G. F. Strouse, *J. Am. Chem. Soc.*, 2004, **126**, 7063–7070.
19 A. M. Smith and S. Nie, *Acc. Chem. Res.*, 2010, **43**, 190–200.
20 M. V. Kovalenko, L. Manna, A. Cabot, Z. Hens, D. V. Talapin, C. R. Kagan, V. I. Klimov, A. L. Rogach, P. Reiss, D. J. Milliron, P. Guyot-Sionnnest, G. Konstantatos, W. J. Parak, T. Hyeon, B. A. Korgel, C. B. Murray and W. Heiss, *ACS Nano*, 2015, **9**, 1012–1057.
21 Y. Yang, H. Qin, M. Jiang, L. Lin, T. Fu, X. Dai, Z. Zhang, Y. Niu, H. Cao, Y. Jin, F. Zhao and X. Peng, *Nano Lett.*, 2016, **16**, 2133–2138.
22 G. Palui, F. Aldeek, W. Wang and H. Mattoussi, *Chem. Soc. Rev.*, 2015, **44**, 193–227.
23 A. Fedosyuk, A. Radchanka, A. Antanovich, A. Prudnikau, M. V. Kvach, V. Shmanai and M. Artemyev, *Langmuir*, 2016, **32**, 1955–1961.
24 M. A. Boles and D. V. Talapin, *J. Am. Chem. Soc.*, 2014, **136**, 5868–5871.
25 J. Y. Woo, S. Lee, S. Lee, W. D. Kim, K. Lee, K. Kim, H. J. An, D. C. Lee and S. Jeong, *J. Am. Chem. Soc.*, 2016, **138**, 876–883.
26 J. C. Flanagan and M. Shim, *J. Phys. Chem. C*, 2015, **119**, 20162–20168.
27 D. J. Weinberg, C. He and E. A. Weiss, *J. Am. Chem. Soc.*, 2016, **138**, 2319–2326.
28 P. R. Brown, D. Kim, R. R. Lunt, N. Zhao, M. G. Bawendi, J. C. Grossman and V. Bulović, *ACS Nano*, 2014, **8**, 5863–5872.
29 S. J. Lim, L. Ma, A. Schleife and A. M. Smith, *Coord. Chem. Rev.*, 2016, **320–321**, 216–237.
30 Z. Li and X. Peng, *J. Am. Chem. Soc.*, 2011, **133**, 6578–86.
31 D. Chen, Y. Gao, Y. Chen, Y. Ren and X. Peng, *Nano Lett.*, 2015, **15**, 4477–4482.
32 E. M. Hutter, E. Bladt, B. Goris, F. Pietra, J. C. Van Der Bok, P. Mark, C. D. M. Donegá, S. Bals, D. D. Vanmaekelbergh, M. P. Boneschanscher, C. D. M. Donegá, S. Bals and D. D. Vanmaekelbergh, *Nano Lett.*, 2014, **14**, 6257–6262.
33 J. S. Son, X.-D. Wen, J. Joo, J. Chae, S. Baek, K. Park, J. H. Kim, K. An, J. H. Yu, S. G. Kwon, S.-H. Choi, Z. Wang, Y.-W. Kim, Y. Kuk, R. Hoffmann and T. Hyeon, *Angew. Chemie Int. Ed.*, 2009, **121**, 6993–6996.
34 E. Lhuillier, S. Pedetti, S. Ithurria, B. Nadal, H. Heuclin and B. Dubertret, *Acc. Chem. Res.*, 2015, **48**, 22–30.
35 F. Wang, Y. Wang, Y.-H. Liu, P. J. Morrison, R. A. Loomis and W. E. Buhro, *Acc. Chem. Res.*, 2015, **48**, 13–21.
36 F. Fan, P. Kanjanaboos, M. Saravanapavanantham, E. Beauregard, G. Ingram, E. Yassitepe, M. M. Adachi, O. Voznyy, A. K. Johnston, G. Walters, G.-H. Kim, Z.-H. Lu and E. H. Sargent, *Nano Lett.*, 2015, **15**, 4611–4615.
37 B. Guzelturk, Y. Kelestemur, M. Olutas, S. Delikanli and H. V. Demir, *ACS Nano*, 2014, **8**, 6599–6605.
38 A. W. Achtstein, A. V. Prudnikau, M. V. Ermolenko, L. I. Gurinovich, S. V. Gaponenko, U. Woggon, A. V. Baranov, M. Y. Leonov, I. D. Rukhlenko, A. V. Fedorov and M. V. Artemyev, *ACS Nano*, 2014, **8**, 7678–7686.
39 A. W. Achtstein, A. Schliwa, A. Prudnikau, M. Hardzei, M. V. Artemyev, C. Thomsen and U. Woggon, *Nano Lett.*, 2012, **12**, 3151–3157.
40 C. E. Rowland, I. Fedin, H. Zhang, S. K. Gray, A. O. Govorov, D. V. Talapin and R. D. Schaller, *Nat. Mater.*, 2015, **14**, 484–489.

View Article Online
DOI: 10.1039/C7NR05065H

41 R. Scott, A. W. Achtstein, A. V. Prudnikau, A. Antanovich, L. D. A. Siebbeles, M. Artemyev and U. Woggon, *Nano Lett.*, 2016, **16**, 6576–6583.

42 C. She, I. Fedin, D. S. Dolzhnikov, P. D. Dahlberg, G. S. Engel, R. D. Schaller and D. V. Talapin, *ACS Nano*, 2015, **9**, 9475–9485.

43 M. Olutas, B. Guzelturk, Y. Kelestemur, A. Yeltik, S. Delikanli and H. V. Demir, *ACS Nano*, 2015, **9**, 5041–5050.

44 A. W. Achtstein, A. Antanovich, A. Prudnikau, R. Scott, U. Woggon and M. Artemyev, *J. Phys. Chem. C*, 2015, **119**, 20156–20161.

45 S. Ithurria and D. V. Talapin, *J. Am. Chem. Soc.*, 2012, **134**, 18585–18590.

46 A. Prudnikau, A. Chuvilin and M. V. Artemyev, *J. Am. Chem. Soc.*, 2013, **135**, 14476–14479.

47 A. V. Antanovich, A. V. Prudnikau, D. Melnikau, Y. P. Rakovich, A. Chuvilin, U. Woggon, A. W. Achtstein and M. V. Artemyev, *Nanoscale*, 2015, **7**, 8084–8092.

48 B. Guzelturk, O. Erdem, M. Olutas, Y. Kelestemur and H. V. Demir, *ACS Nano*, 2014, **8**, 12524–12533.

49 S. Jana, M. de Frutos, P. Davidson and B. Abécassis, *Sci. Adv.*, 2017, **3**, e1701483.

50 A. Antanovich, A. Prudnikau, A. Matsukovich, A. Achtstein and M. Artemyev, *J. Phys. Chem. C*, 2016, **120**, 5764–5775.

51 S. Ithurria and B. Dubertret, *J. Am. Chem. Soc.*, 2008, **130**, 16504–5.

52 B. Fritzinger, R. K. Capek, K. Lambert, J. C. Martins and Z. Hens, *J. Am. Chem. Soc.*, 2010, **132**, 10195–10201.

53 R. Gomes, A. Hassinen, A. Szczygiel, Q. Zhao, A. Vantomme, J. C. Martins and Z. Hens, *J. Phys. Chem. Lett.*, 2011, **2**, 145–152.

54 J. S. Owen, J. Park, P.-E. Trudeau and A. P. Alivisatos, *J. Am. Chem. Soc.*, 2008, **130**, 12279–12281.

55 R. R. Knauf, J. C. Lennox and J. L. Dempsey, *Chem. Mater.*, 2016, **28**, 4762–4770.

56 P. Schapotschnikow, B. Hommersom and T. J. H. Vlugt, *J. Phys. Chem. C*, 2009, **113**, 12690–12698.

57 S. F. Wuister, C. de Mello Donegá and A. Meijerink, *J. Phys. Chem. B*, 2004, **108**, 17393–17397.

58 J. Q. Grim, S. Christodoulou, F. Di Stasio, R. Krahne, R. Cingolani, L. Manna and I. Moreels, *Nat. Nanotechnol.*, 2014, **9**, 891–895.

59 J. J. Buckley, E. Couderc, M. J. Greaney, J. Munteanu, C. T. Riche, S. E. Bradforth and R. L. Brutchey, *ACS Nano*, 2014, **8**, 2512–2521.

60 M. T. Frederick and E. A. Weiss, *ACS Nano*, 2010, **4**, 3195–3200.

61 A. W. Achtstein, R. Scott, S. Kickhöfel, S. T. Jagsch, S. Christodoulou, G. H. V. Bertrand, A. V. Prudnikau, A. Antanovich, M. Artemyev, I. Moreels, A. Schliwa and U. Woggon, *Phys. Rev. Lett.*, 2016, **116**, 116802.

62 E. B. Ituen, J. E. Asuquo and O. R. Ogede, *Int. J. Comput. Theor. Chem.*, 2014, **2**, 14.

63 J. de Araújo Gonçalves, A. L. D. Ramos, L. L. L. Rocha, A. K. Domingos, R. S. Monteiro, J. S. Peres, N. C. Furtado, C. A. Taft and D. A. G. Aranda, *J. Phys. Org. Chem.*, 2011, **24**, 54–64.

64 Y. Zhou, F. Wang and W. E. Buhro, *J. Am. Chem. Soc.*, 2015, **137**, 15198–15208.

65 S. A. Cherevkov, A. V. Fedorov, M. V. Artemyev, A. V. Prudnikau and A. V. Baranov, *Phys. Rev. B - Condens. Matter Mater. Phys.*, 2013, **88**, 41303.

66 R. Benchamekh, N. A. Gippius, J. Even, M. O. Nestoklon, J.-M. Jancu, S. Ithurria, B. Dubertret, A. L. Efros and P. Voisin, *Phys. Rev. B*, 2014, **89**, 35307.

67 A. M. Smith, A. M. Mohs and S. Nie, *Nat. Nanotechnol.*, 2009, **4**, 56–63.

68 S. H. Tolbert and A. P. Alivisatos, *Annu. Rev. Phys. Chem.*, 1995, **46**, 595–626.

69 L. Jing, S. V Kershaw, T. Kipp, S. Kalytchuk, K. Ding, J. Zeng, M. Jiao, X. Sun, A. Mews, A. L. Rogach and M. Gao, *J. Am. Chem. Soc.*, 2015, **137**, 2073–2084.

70 J. Rockenberger, L. Tröger, A. L. Rogach, M. Tischer, M. Grundmann, A. Eychmüller and H. Weller, *J. Chem. Phys.*, 1998, **108**, 7807–7815.

71 R. W. Meulenberg, T. Jennings and G. F. Strouse, *Phys. Rev. B*, 2004, **70**, 235311.

72 S. Ithurria, M. D. Tessier, B. Mahler, R. P. S. M. Lobo, B. Dubertret and A. L. Efros, *Nat. Mater.*, 2011, **10**, 936–941.

73 W. I. F. David, *J. Appl. Crystallogr.*, 1986, **19**, 63–64.

74 M. Wojdyr, *J. Appl. Crystallogr.*, 2010, **43**, 1126–1128.

75 C. L. McGuiness, D. Blasini, J. P. Masejewski, S. Uppili, O. M. Cabarcos, D. Smilgies and D. L. Allara, *ACS Nano*, 2007, **1**, 30–49.

76 D. D. Lovingood, R. Achey, A. K. Paravastu and G. F. Strouse, *J. Am. Chem. Soc.*, 2010, **132**, 3344–3354.

77 S. F. Bent, *ACS Nano*, 2007, **1**, 10–12.

78 S. M. Han, W. R. Ashurst, C. Carraro and R. Maboudian, *J. Am. Chem. Soc.*, 2001, **123**, 2422–2425.

79 T. Ishizaki, N. Saito, L. SunHyung, K. Ishida and O. Takai, *Langmuir*, 2006, **22**, 9962–9966.

80 N. C. Anderson, M. P. Hendricks, J. J. Choi and J. S. Owen, *J. Am. Chem. Soc.*, 2013, **135**, 18536–18548.

81 C. Fang, Z. Chen, X. Liu, Y. Yang, M. Deng, L. Weng, Y. Jia and Y. Zhou, *Inorganica Chim. Acta*, 2009, **362**, 2101–2107.

82 N. Stock and T. Bein, *J. Mater. Chem.*, 2005, **15**, 1384–1391.

83 J. Tao, M.-L. Tong and X.-M. Chen, *J. Chem. Soc. Dalt. Trans.*, 2000, 3669–3674.

84 W. Clegg, J. T. Cressey, A. McCamley and B. P. Straughan, *Acta Crystallogr. Sect. C Cryst. Struct. Commun.*, 1995, **51**, 234–235.

85 W. Shan, W. Walukiewicz, J. W. Ager, K. M. Yu, J. Wu and E. E. Haller, *Appl. Phys. Lett.*, 2004, **84**, 67–69.

86 F. Gindele, U. Woggon, W. Langbein, J. M. Hvam, K. Leonardi, D. Hommel and H. Selke, *Phys. Rev. B*, 1999, **60**, 8773–8782.

87 Basu P. K., *Theory of Optical Processes in Semiconductors: Bulk and Microstructures*, Clarendon Press, New York, 1st edn., 1998.

88 M. Willatzen, M. Cardona and N. E. Christensen, *Phys. Rev. B*, 1995, **51**, 17992–17994.

89 R. Scott, A. W. Achtstein, A. Prudnikau, A. Antanovich, S. Christodoulou, I. Moreels, M. Artemyev and U. Woggon,

View Article Online
DOI: 10.1039/C7NR05065H

Nano Lett., 2015, **15**, 4985–4992.